A multiresolution fusion framework based on probabilistic graphical modeling for burnt zones mapping from satellite and UAV imagery

Martina Pastorino, Gabriele Moser, Fabien Guerra, Sebastiano B Serpico, Josiane Zerubia

A MULTIRESOLUTION FUSION FRAMEWORK BASED ON PROBABILISTIC GRAPHICAL MODELING FOR BURNT ZONES MAPPING FROM SATELLITE AND UAV IMAGERY

Martina Pastorino[1,2], Gabriele Moser[1], Fabien Guerra[3], Sebastiano B. Serpico[1], and Josiane Zerubia[2]

[1] University of Genoa, DITEN dept., Genoa, Italy, martina.pastorino@edu.unige.it.
[2] Inria, Université Côte d'Azur, Sophia-Antipolis, France.
[3] INRAE, RECOVER, Aix-Marseille University, Aix-en-Provence, France

ABSTRACT

This paper tackles the semantic segmentation of zones affected by forest fires by the introduction of methods fusing multimodal imagery collected from unmanned aerial vehicles (UAVs) and satellite platforms. The multiresolution fusion task is especially challenging in this case because the difference between the involved spatial resolutions is very large – a situation that is normally not addressed by traditional multiresolution schemes. Two novel multiresolution fusion approaches, based on Bayesian and probabilistic graphical fusion models and integrated with a deep fully convolutional network and with the expectation-maximization algorithm, are proposed. The application is to a real case of fire zone mapping and management in the area of Marseille, France.

***Index Terms*—** Semantic segmentation, satellite images, UAV, probabilistic fusion, fires

1. INTRODUCTION

The increasing occurrence of wildfires, amplified by the changing climate conditions and drought, has significant impacts on natural resources, ecosystem responses, and climate change [1]. In this framework, deriving the extent of areas affected by wildfires is critical to fire management, protection of the population, damage assessment, and better understanding of the consequences of fires. Burnt area mapping is crucial not only to prevent further damage but also to manage the area itself. Reliable damage assessment often requires field measurements, which might be inaccessible in some poorly managed areas [2] other than time-consuming.

Thanks to the current availability of Earth observation satellites, such as the Sentinel-2 MultiSpectral Instrument (MSI) and Landsat 8 and 9, it is possible to have access to data for the monitoring and the mapping of the burnt areas. In the past two decades, several algorithms utilizing remote sensing satellite data have been developed to map fire-affected areas [3]. Multispectral channels, especially in the near and short-wave infrared (NIR, SWIR) wavelength ranges, are commonly used in burnt area mapping [4].

In recent years, unmanned aerial vehicles (UAV), or drones, have also been widely used in forest fire monitoring, thanks to their high flexibility, low-cost, and ability to cover wide areas during the day or night [5]. On one hand, the spatial resolution granted by UAVs is usually very high. On the other hand, fires captured by UAVs are typically characterized by a small area coverage, irregular contours, complex scene background, and susceptibility to forest cover, making the accurate segmentation of burnt areas challenging [6].

At the same time, satellite-based monitoring provides an efficient and large-scale wildfire assessment due to its wide range, time frequency and accuracy. However, this approach suffers from aerosol and cloud occlusions, which can make forest fires hardly detectable [7], and generally allows for much coarser spatial resolutions than through UAVs.

In recent years, deep learning-based methods have been introduced for monitoring forest fires thanks to their state-of-the-art performance on computer vision tasks [7, 8, 9] and their ability to detect patterns in complex data by automatically learning from examples [3]. Models based on CNNs [3, 10, 11, 12] and on transformers [13] have been applied to several segmentation problems [5, 14, 15]. However, deep learning models require a large number of labeled images, which may not always be available, other than costly and time-consuming to generate [3, 7].

The joint availability of satellite and UAV acquisitions of zones affected by wildfires, with their complementary features, presents a huge potential for the mapping and monitoring of burnt areas and, at the same time, a big challenge for the development of a classifier capable to fully take advantage of this multimodal information.

In this paper, to address the huge contrast between the resolutions of the available input image sources, two novel methods combining stochastic modeling and decision fusion, and integrated with a deep fully convolutional network (FCN) and with the expectation-maximization algorithm are presented.

2. METHODOLOGY

2.1. Pixelwise probabilistic fusion

The first developed method aims to fuse the information at different resolutions in a pixelwise probabilistic framework. The idea is to extract the thematic information contained in

the two acquisitions collected by the different sensors (at very different spatial resolutions and with generally different spectral bands) separately, and perform a posterior probability pixelwise decision fusion [16]. Let us denote as $\mathcal{X}$ a patch of the image at finer resolution acquired by the drone, with size corresponding exactly to one pixel in the coarser resolution lattice associated with the satellite acquisition. Let $\tilde{x}$ be the feature vector of this pixel. This underlies the assumption that the UAV and satellite images are well registered, so that one pixel in the latter corresponds to a patch of $D \times D$ pixels in the former. Accordingly, D represents the resolution ratio associated with the input multiresolution dataset. For example, if the spatial resolutions of the UAV and satellite images are of the order of a few centimeters and of a few meters or tens of meters, respectively, D is expected to range in the hundreds.

For training purposes, the first proposed method requires the definition of a ground truth (GT) at the coarser level, starting from an input GT map, which we assume available for the drone acquisition at the finer resolution. This GT map at the UAV resolution is assumed to include two classes, "burnt" (ω_1) and "non-burnt" (ω_2). Let y_i be the label of the ith pixel of the $D \times D$ patch at the finer (UAV) resolution and let $\tilde{y}$ be the corresponding class membership at the coarser resolution. The coarser resolution GT is created with the following rules:

1. if $y_i = \omega_1, \forall i \in D \times D$, then $\tilde{y} = \psi_1$ ("burnt").
2. if $y_i = \omega_2, \forall i \in D \times D$, then $\tilde{y} = \psi_2$ ("non-burnt").
3. else, $\tilde{y}$ belongs to a third class ψ_3 ("partially burnt").

Accordingly, the two resolution levels correspond to distinct sets of classes: $\Omega = \{\omega_1, \omega_2\}$ on the finer resolution lattice of the UAV image and $\tilde{\Omega} = \{\psi_1, \psi_2, \psi_3\}$ on the coarser resolution grid of the satellite image.

The pixelwise probabilistic fusion is formalized as follows in terms of decision fusion from suitable input posteriors. Specifically, the posterior distribution of y_i given all available input information, i.e., given the random field $\mathcal{X}$ in the $D \times D$ crop at the UAV resolution and the feature vector $\tilde{x}$ at the satellite image resolution, can be expressed as:

$$P(y_i|\mathcal{X}, \tilde{x}) = \sum_{\tilde{y} \in \tilde{\Omega}} P(y_i, \tilde{y}|\mathcal{X}, \tilde{x}). \tag{1}$$

Under suitable conditional independence assumptions, widely accepted in the development of Bayesian and Markovian approaches (e.g., in [17, 18, 19]), and applying the Bayes theorem, we can prove that (1) implies:

$$P(y_i|\mathcal{X}, \tilde{x}) \propto \sum_{\tilde{y} \in \tilde{\Omega}} P(y_i|\mathcal{X}) P(\tilde{y}|\tilde{x}) \frac{P(y_i|\tilde{y})}{P(y_i)} \tag{2}$$

where $P(y_i|\mathcal{X})$ is the posterior probability of the acquisition at finer spatial resolution conditioned on all UAV feature vectors in the $D \times D$ patch, $P(\tilde{y}|\tilde{x})$ is the posterior probability computed for the satellite acquisition at coarser spatial resolution on the individual pixel corresponding to the patch, $P(y_i)$ is the prior probability of the class labels at the finer resolution, and $P(y_i|\tilde{y})$ is the conditional probability of the labels at the finer resolution given the ones at the coarser resolution. Given the size of the input multiscale information, the image at the finer resolution is processed with an FCN and the posterior probability $P(y_i|\mathcal{X})$ is the output of the softmax layer of the FCN when the $D \times D$ patch of UAV data is fed as input. On the contrary, the posterior probability $P(\tilde{y}|\tilde{x})$ of the coarser resolution image is predicted with random forest (RF). $P(y_i)$ is estimated as the relative frequency in the training set considered. In particular, the joint distribution $P(y_i, \tilde{y})$ is assumed stationary within the patch, i.e., $\theta_{k,h} = P(y_i = \omega_k, \tilde{y} = \psi_h)$ ($k = 1, 2; h = 1, 2, 3$) is assumed independent from the pixel location i within the patch.

Considering the discrepancy in the number of classes between the GT at the finer and coarser resolutions, the conditional probability distribution $P(y_i|\tilde{y})$ between the labels of the two multiresolution images is defined indirectly by the vector θ collecting the aforementioned joint probabilities $\theta_{k,h}$ ($k = 1, 2; h = 1, 2, 3$). In the proposed method, these parameters are estimated through an approximate formulation of the expectation maximization (EM) algorithm [20, 21]. EM is an iterative parameter estimation techniques for problems characterized by data incompleteness and converging, under suitable assumptions, to maximum-likelihood estimates [22]. Denoting as θ^t the estimate computed for θ at the tth iteration, the EM formulation within the proposed technique is defined by the following iterative equations ($t = 0, 1, 2, \ldots$):

$$\begin{cases} \alpha^t_{i,k,h} = P(y_i = \omega_k|\mathcal{X}) P(\tilde{y} = \psi_h|\tilde{x}) \frac{\theta^t_{k,h}}{\sum_l \theta^t_{k,l} \sum_l \theta^t_{l,h}} \\ \theta^{t+1}_{k,h} \propto \sum_i \alpha^t_{i,k,h} \\ \sum_{k,h} \theta^{t+1}_{k,h} = 1 \end{cases} \tag{3}$$

where the posteriors in the first equation are predicted through FCN and RF models, as mentioned before, and where the initialization θ^0 corresponds to a uniform joint label distribution.

2.2. Multiresolution fusion through hierarchical probabilistic graphical model

The key idea of the second method is to fuse the multiresolution information through a pyramidal tree structure, where the information is inserted at its native resolution [23]. In this case, the root layer contains the coarse resolution satellite data and the leaf layer contains the fine resolution UAV imagery.

Given the relationship $1 : D$ between the two resolutions and the expected order of magnitude of D, it would possibly require tens of levels in order to maintain the standard power-of-two relationship typical of traditional pyramidal graphs with quadtree topologies, making the inference very computationally expensive. Therefore, the proposed hierarchical probabilistic graphical model (PGM) formulation

introduces a partially irregular quadtree. The leaf layer, where UAV data are stored, is interpreted as the Lth layer of the quadtree. First, starting from this leaf layer, intermediate layers $L-1,\dots,1$ are constructed as in a traditional quadtree, by progressively halving the spatial resolution, and by associating downsampled UAV image data. The coarsest resolution that is obtained in this way corresponds to level 1 and is 2^{L-1} times coarser than that of the UAV image. The root, i.e., the 0th layer of the tree with which the satellite data are associated, is linked directly to level 1.

Differently from a conventional quadtree, here, many more connections are present. Indeed, each pixel at the root corresponds to a patch of $(2^{1-L}D)\times(2^{1-L}D)$ pixels on level 1: all such pixels are connected to the single pixel on the root. This obviously affects the formulation of marginal posterior mode (MPM) inference criterion and the flow of information across the top-down and bottom-up levels.

A hierarchical MRF is defined over this quadtree. Using the same notations as in Section 2.1 and calling x_i the feature vector of the i-th pixel of the drone patch and S^ℓ the ℓth layer of the described tree, the MPM criterion is extended as follows. Firstly, a top-down pass to compute the prior probability of the class label, starting from the root to the leaves is performed:

$$P(y_i)=\sum_{y_i^-\in\Omega} P(y_i|y_i^-)P(y_i^-) \quad i\in S^\ell,\ell\geq 1 \tag{4}$$

For level $\ell=1$ in the quadtree, the equation relates to the root layer, thus becoming:

$$P(y_i)=\sum_{\tilde{y}\in\tilde{\Omega}} P(y_i|\tilde{y})P(\tilde{y}) \quad i\in S^1 \tag{5}$$

For the root layer, these probabilities are initialized as the relative frequencies of the classes in the training set. Secondly, a bottom-up pass to compute the probability of having a certain class label y_i on pixel i, given the observation of the descendants x_i^d of i in the tree is performed:

$$P(y_i|x_i^d)\propto P(y_i|x_i)\prod_{t\in i^+}\sum_{y_t\in\Omega}\frac{P(y_t|x_t^d)P(y_t|y_i)}{P(y_t)}, \tag{6}$$

$$P(y_i|y_i^c,x_i^d)\propto\frac{P(y_i|x_i^d)P(y_i|y_{i^-})P(y_{i^-})}{P(y_i)^{n_i}}$$

with y_i^c collecting the labels of all sites connected to i, and n_i is the number of such sites. Finally, a second top-down pass from the root (i.e., the pixel grid related to the satellite image) to the leaves is performed. Starting from level $\ell=1$:

$$P(y_i|\mathcal{X},\tilde{x})=\sum_{y_i^c\in\Omega^{n_i}} P(y_i^c|y_i,x_i^d)P(\tilde{y}|\mathcal{X},\tilde{x}), \quad i\in S^1 \tag{7}$$

where, in this case, y_i^c also includes $\tilde{y}$. Then, we move to the lower levels of the tree ($i\in S^\ell,\ell\geq 1$):

$$P(y_i|\mathcal{X},\tilde{x})=\sum_{y_i^c\in\Omega^{n_i}} P(y_i^c|y_i,x_i^d)P(y_{i^-}|\mathcal{X},\tilde{x}) \tag{8}$$

with $i\in S^\ell,\ell=2,3,\dots,L$. The transition probability $P(y_i|y_i^-)$ across consecutive scales is defined through a parametric stationary model [24].

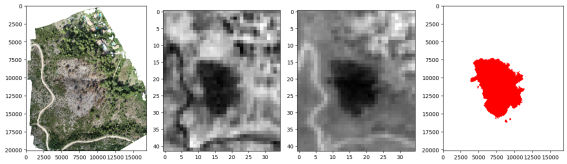

(a) (b) (c) (d)

Fig. 1: **Input images:** (a) drone image, (b) NDVI Sentinel-2 image, (c) NIR Sentinel-2 image, and (d) the GT with the same resolution of the drone image. Class legend: burnt (red) and non-burnt (white).

3. EXPERIMENTAL VALIDATION

The study area is La Destrousse, a commune in the department of Bouches-du-Rhône, Provence-Alpes-Côte d'Azur, France. The dataset includes an RGB image of size 16904×20324 pixels acquired by an UAV with a spatial resolution of about 2 cm. In the annotation of the GT, the boundaries of the burnt area were found with the canopy height model (CHM), which measures the height of trees, buildings, and other structures above the ground topography [25, 26, 27].

To integrate the available information with data at different spectral bands, useful to discriminate burnt areas from non-burnt zones, the NIR channels of a Sentinel-2 image were used. These channels have a spatial resolution of 10 m (see Fig. 1). The drone image was acquired shortly after the fire of 11 July 2018 and the first available Sentinel-2 data of the same zone is dated 14 July 2018.

Given the relationship between the two spatial resolutions, in this case $D=480$. To maintain a reasonable number of levels and, simultaneously, to model multiscale information, the drone imagery was resized to 4 cm and 8 cm of resolution (i.e., $L=3$). Hence, each Sentinel-2 pixel is the parent pixel of the 14400 pixels of the layer at 8 cm of resolution (with size 120×120 pixels). The dataset was properly split in separate zones representing the training and test sets.

The proposed methods were compared with the baseline U-Net trained on the UAV data and with a multiresolution fusion architecture solely based on deep learning. In this architecture, the coarser resolution data were included directly in the first convolutional layers as a bias scalar term, obtained multiplying the channel information of the pixel $\tilde{x}$ by a learnable weighting vector. To our knowledge, the proposed approaches are the first ones combining UAV and Sentinel-2 im-

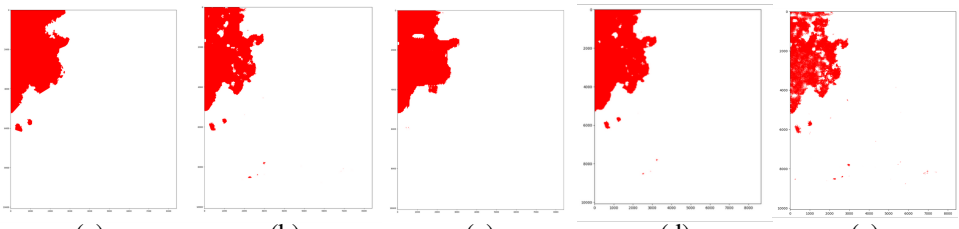

(a) (b) (c) (d) (e)

Fig. 2: **GT and classification results:** (a) GT and result of the (b) U-Net trained on UAV data, (c) first proposed method fusing UAV and Sentinel-2 data, (d) second proposed approach, including the bottom-up and the top-down passes, and (e) deep learning multiresolution fusion used for comparison. Class legend: burnt (red) and non-burnt (white).

Table 1: Classification accuracies of the proposed methods and of the comparison techniques.

Architecture	False alarm rate	Missed alarm rate	Overall error rate
U-Net (on UAV)	0.28	10.81	1.61
DL multires. fusion	**0.19**	27.08	3.51
First prop. method	0.48	8.55	1.47
Second prop. method	**0.19**	**7.43**	**1.17**

ages at their native resolutions for burnt area mapping, therefore comparisons with state-of-the-art methods developed for this specific task were not possible.

Table 1 presents the results obtained by the proposed methods and the two comparison techniques in terms of false and missed alarm rates, and overall error rate with respect to a test map (annotated as the aforementioned training map). The quantitative results suggest the overall effectiveness of the FCN baseline on the UAV image to estimate the burnt and non-burnt areas, with an overall error rate of 1.61%. These results are visually confirmed by the classification map shown in Fig. 2(b), which appears to follow the outline of the original GT, yet being characterized by several missed alarms in between the burnt area.

With respect to the original results achieved by the FCN only on the drone image, the proposed pixelwise probabilistic fusion combining RGB and multispectral images presents slightly more accurate results in terms of overall error rate and missed alarm rate, and a 0.2% loss in terms of the false alarm rate. The classification map (shown in Fig. 2(c)) appears to be more accurate and significantly visually smoother as compared to the previous result (shown in Fig. 2(b)), thanks to the incorporation of the Sentinel-2 image.

The reported results of the second proposed method are obtained after the second top-down pass, thus taking into account all the information of the observation of the descendant pixels and the labels of all the connected pixels (in this case, the parent pixels). The overall error rate of this second method is of about 1%, with the lowest false and missed alarm rates. The classwise accuracies are higher for the non-burnt zones, which are a majority class with respect to the "burnt" class. The classification map shown in Fig. 2(d) suggests the potential of this proposed model, as the map appears to be visually smooth and accurate, especially in comparison with the original GT, outperforming not only the baseline but also the previous fusion method in the detection of the burnt area.

Concerning the other comparison method, the neural architecture, the classification map shown in Fig. 2(e) appears to reproduce rather accurately the GT, as it is also suggested by the results in terms of overall error rate and missed / false alarms. Nevertheless, the results are suboptimal with respect to the ones achieved by the proposed approaches.

4. DISCUSSION AND CONCLUSION

In this paper, two probabilistic fusion methods were proposed for the joint use of multiresolution and multiband information for the semantic segmentation of zones affected by fires with UAV and satellite images. The resulting multiresolution task is quite extreme, since the resolution ratio between the input image sources is of the order of the hundreds.

The experimental validation suggests the effectiveness of the proposed methods for the semantic segmentation of zones affected by fires. The two methods obtain accurate classification results and maps, in particular by the second proposed approach, fusing multiresolution information through an irregular quadtree topology and a hierarchical PGM. This confirms the potential of the combination of FCN architectures with PGMs on appropriate graphs.

Future developments will involve the application to different case studies related to forest fires with data acquired by different sensors and at different resolutions, possibly containing additional spectral information to compute application-specific meaningful indices like the normalized burn ratio (NBR) [28]. Furthermore, it would be interesting to integrate the proposed method with transfer learning and test it with fire image data characterized by different features and associated with different geographical areas.

5. REFERENCES

[1] D. Bowman, G. Williamson, J. Abatzoglou, C. Kolden, M. Cochrane, and A. Smith, "Human exposure and sensitivity to globally extreme wildfire events," *Nat. Ecol. Evol.*, vol. 1, no. 3, pp. 58, February 2017.

[2] D. Bowman, "Wildfire science is at a loss for comprehensive data," *Nature*, vol. 560, pp. 07–07, 08 2018.

[3] D. Rashkovetsky, F. Mauracher, M. Langer, and M. Schmitt, "Wildfire detection from multisensor satellite imagery using deep semantic segmentation," *IEEE J. Sel. Top. Appl. Earth Obs. Remote Sens.*, vol. 14, pp. 7001–7016, 2021.

[4] X. Hu, P. Zhang, and Y. Ban, "Large-scale burn severity mapping in multispectral imagery using deep semantic segmentation models," *ISPRS J. Photogramm. Remote Sens.*, vol. 196, pp. 228–240, 2023.

[5] R. Ghali, M. Akhloufi, and W. Mseddi, "Deep learning and transformer approaches for UAV-based wildfire detection and segmentation," *Sensors*, vol. 22, 03 2022.

[6] L. Zhang, M. Wang, Y. Ding, T. Wan, B. Qi, and Y. Pang, "FBC-ANet: A semantic segmentation model for UAV forest fire images combining boundary enhancement and context awareness," *Drones*, vol. 7, no. 7, 2023.

[7] J. Wang, X. Fan, X. Yang, T. Tjahjadi, and Y. Wang, "Semi-supervised learning for forest fire segmentation using UAV imagery," *Forests*, vol. 13, no. 10, 2022.

[8] E. Tsalera, A. Papadakis, I. Voyiatzis, and M. Samarakou, "CNN-based, contextualized, real-time fire detection in computational resource-constrained environments," *Energy Rep.*, vol. 9, pp. 247–257, 2023.

[9] F. Zhao, R. Sun, L. Zhong, R. Meng, C. Huang, X. Zeng, M. Wang, Y. Li, and Z. Wang, "Monthly mapping of forest harvesting using dense time series Sentinel-1 SAR imagery and deep learning," *Remote Sens. Environ.*, vol. 269, pp. 112822, 2022.

[10] P. Pozzobon de Bem, O. Abílio de C. Júnior, O. Luiz Ferreira de Carvalho, R. Arnaldo Trancoso Gomes, and R. Fontes Guimarães, "Performance analysis of deep convolutional autoencoders with different patch sizes for change detection from burnt areas," *Remote Sens.*, vol. 12, no. 16, 2020.

[11] G. Henrique de Almeida Pereira, A. Minoro Fusioka, B. Tomoyuki Nassu, and R. Minetto, "Active fire detection in Landsat-8 imagery: A large-scale dataset and a deep-learning study," *ISPRS J. Photogramm. Remote Sens.*, vol. 178, pp. 171–186, 2021.

[12] S. Teymoor Seydi, M. Hasanlou, and J. Chanussot, "DSMNN-Net: A deep siamese morphological neural network model for burned area mapping using multispectral Sentinel-2 and hyperspectral PRISMA images," *Remote Sens.*, vol. 13, pp. 5138, 2021.

[13] A. Vaswani, N. Shazeer, N. Parmar, J. Uszkoreit, L. Jones, A. N. Gomez, L. Kaiser, and I. Polosukhin, "Attention is all you need," in *Adv. Neural Inf. Process. Syst.*, 2017.

[14] T. F.R. Ribeiro, F. Silva, J. Moreira, and R. L. de C. Costa, "Burned area semantic segmentation: A novel dataset and evaluation using convolutional networks," *ISPRS J. Photogramm. Remote Sens.*, vol. 202, pp. 565–580, 2023.

[15] Z. Shirvani, O. Abdi, and R. C. Goodman, "High-resolution semantic segmentation of woodland fires using residual attention U-Net and time series of Sentinel-2," *Remote Sens.*, vol. 15, no. 5, 2023.

[16] G.J. Briem, J.A. Benediktsson, and J.R. Sveinsson, "Multiple classifiers applied to multisource remote sensing data," *IEEE Trans. Geosci. Remote. Sens.*, vol. 40, no. 10, pp. 2291–2299, 2002.

[17] Z. Kato and J. Zerubia, "Markov random fields in image segmentation," *Found. Trends Signal Process.*, vol. 5, no. 1-2, pp. 1–155, 2012.

[18] S. Z. Li, *Markov random field modeling in image analysis*, Springer, 3rd edition, 2009.

[19] J. M. Laferté, P. Pérez, and F. Heitz, "Discrete Markov image modeling and inference on the quadtree," *IEEE Trans. Image Process.*, vol. 9, no. 3, pp. 390–404, 2000.

[20] T.K. Moon, "The expectation-maximization algorithm," *IEEE Signal Process. Mag.*, vol. 13, no. 6, pp. 47–60, 1996.

[21] A. P. Dempster, N. M. Laird, and D. B. Rubin, "Maximum likelihood from incomplete data via the EM algorithm," *J. R. Stat. Soc. Series B (Stat. Methodol.)*, vol. 39, no. 1, pp. 1–38, 1977.

[22] R. A. Redner and H. F. Walker, "Mixture densities, maximum likelihood and the EM algorithm," *SIAM Review*, vol. 26, no. 2, pp. 195–239, 1984.

[23] M. Pastorino, G. Moser, S. B. Serpico, and J. Zerubia, "Semantic segmentation of remote-sensing images through fully convolutional neural networks and hierarchical probabilistic graphical models," *IEEE Trans. Geosci. Remote Sens.*, vol. 60, no. 5407116, pp. 1–16, 2022.

[24] C. A. Bouman and M. Shapiro, "A multiscale random field model for Bayesian image segmentation," *IEEE Trans. Image Process.*, vol. 3, no. 2, pp. 162–177, 1994.

[25] J. P. Dandois and E. C. Ellis, "High spatial resolution three-dimensional mapping of vegetation spectral dynamics using computer vision," *Remote Sens. Environ.*, vol. 136, pp. 259–276, 2013.

[26] J. Hyyppä, H. Hyyppä, D. Leckie, F. Gougeon, X. Yu, and M. Maltamo, "Review of methods of small-footprint airborne laser scanning for extracting forest inventory data in boreal forests," *Int. J. Remote Sens.*, vol. 29, no. 5, pp. 1339–1366, 2008.

[27] N. Lang, W. Jetz, K. Schindler, and J. D. Wegner, "A high-resolution canopy height model of the Earth," *Nat. Ecol. Evol.*, 2023.

[28] K. S. Mpakairi, S. L. Kadzunge, and H. Ndaimani, "Testing the utility of the blue spectral region in burned area mapping: Insights from savanna wildfires," *Remote Sens. Appl. Soc. Environ.*, vol. 20, pp. 100365, 2020.